Effect of Liquid Electrolyte Soaking on the Interfacial Resistance of $Li_7La_3Zr_2O_{12}$ for All-Solid-State Lithium Batteries

Münir M. Besli,[a,b] Camille Usubelli,[a,c] Michael Metzger,[a] Vikram Pande,[a] Katherine Harry,[d] Dennis Nordlund,[e] Sami Sainio,[e] Jake Christensen,[a] Marca M. Doeff,[f,*] Saravanan Kuppan[a,*]

[a]Robert Bosch LLC, Research and Technology Center, Sunnyvale, California 94085, United States
[b]Dept. of Mech. Engineering, Karlsruhe Institute of Technology (KIT), Karlsruhe 76131, Germany
[c]Institute of Physics and Chemistry of Materials of Strasbourg (IPCMS), UMR 7504 CNRS, University of Strasbourg, Strasbourg Cedex 2 67034, France
[d]Holo, Inc., Oakland, California 94607, United States
[e]Stanford Synchrotron Radiation Lightsource, SLAC National Accelerator Laboratory, Menlo Park, California 94025, United States
[f]Lawrence Berkeley National Laboratory, Energy Storage and Distributed Resources Division, University of California, Berkeley, California 94720, United States

*Correspondence and requests for materials should be addressed to M.D. (mmdoeff@lbl.gov) and S.K. (saravanan.kuppan@us.bosch.com)

Key Words

LLZO, all-solid-state battery, lithium-ion battery, garnets, interfacial resistance

Abstract

The impact of liquid electrolyte soaking on the interfacial resistance between garnet structured $Li_7La_3Zr_2O_{12}$ (LLZO) solid electrolyte and metallic lithium has been studied. Lithium carbonate (Li_2CO_3) formed by inadvertent exposure of LLZO to ambient conditions, is generally known to increase interfacial impedance and decrease lithium wettability. Soaking LLZO powders and pellets in electrolyte containing lithium tetrafluoroborate ($LiBF_4$) shows a significantly reduced interfacial resistance and improved contact between lithium and LLZO. Raman spectroscopy, X-ray diffraction (XRD), and soft X-ray absorption spectroscopy (XAS) reveal how Li_2CO_3 is continuously removed with increasing soaking time. On-line mass spectrometry (OMS) and free energy calculations show how $LiBF_4$ reacts with surface carbonate to form carbon dioxide (CO_2). Using a very simple and scalable process that does not involve heat-treatment and expensive

coating techniques, we show that the Li-LLZO interfacial resistance can be reduced by an order of magnitude.

Introduction

Solid-state electrolyte (SSE) systems exhibiting Li^+ conductivities greater than 1 mS/cm at room temperature could potentially enable the use of lithium metal anodes for high energy and high power density batteries,[1–4] but only if they have sufficient chemical stability against lithium metal and can suppress dendrite growth. Li metal anodes offer up to ~50% increase in terms of energy density,[5] and can be combined with state-of-the-art oxide based cathode materials, but also used in emerging battery designs as in Li-air, Li-S and Li-Br batteries.[6–8] However, a number of fundamental issues require a systematic effort to facilitate a commercial product. SSEs such as variants of the garnet-type ceramic oxide $Li_7La_3Zr_2O_{12}$ (LLZO), can exhibit high Li-LLZO interfacial resistances ($R_{Li\text{-}LLZO}$) and poor Li wettability.[9–11] The main sources of this high interfacial impedance are surface contaminants such as Li_2CO_3 and LiOH which form upon air exposure, or are left over from synthesis.[9,12] Also the microstructure of the surface and bulk of the pellet, i.e., ratio of grain boundaries to grains, affects lithium conduction.[11] To lower the interfacial impedances, various methodologies have been suggested in the literature. For example, Cheng et al. used simple polishing papers with different grit numbers to remove an approximately 50 µm thick surface layer.[9] They also suggested heating LLZO at 250 °C under an inert atmosphere to remove lithium carbonate.[13] Yutao et al. proposed to cover LLZO pellets with carbon and fire them at 700 °C, which completely converts Li_2CO_3 to Li_2O and CO and hence removes the undesirable carbonate layer.[14] Han et al. used a surface polishing followed by atomic layer deposition (ALD) of Al_2O_3 to decrease interfacial impedances in LLZO.[15] While all of these methods show improvement to various degrees between the physical interface of Li and garnet-type oxides, each presents potential challenges to large-scale all-solid-state battery (ASSB) manufacturing, especially in terms of compatibility with thin electrolyte layers. Due to the relatively high density and low conductivity of LLZO compared to conventional liquid electrolyte, a separator thickness below 20 um is desired to achieve high energy and power density.[16] Mechanical treatment methods such as polishing may not be applicable at this thickness.

Herein we report a simple and easily scalable method to remove surface carbonate without compromising the mechanical integrity of garnet-type SSEs. Similar to the etching of surface

contaminants on lithium metal surfaces with $LiBF_4$,[17,18] by simply soaking LLZO pellets in organic solvent containing lithium tetrafluoroborate ($LiBF_4$) and subsequent rinsing with organic solvent without salt, we demonstrate that surface contaminants can be removed quickly (Figure 1). This method provides a new, facile, and easily scalable way to clean the surface of garnet-type SSEs and engineer a low interfacial resistance $R_{Li\text{-}LLZO}$.

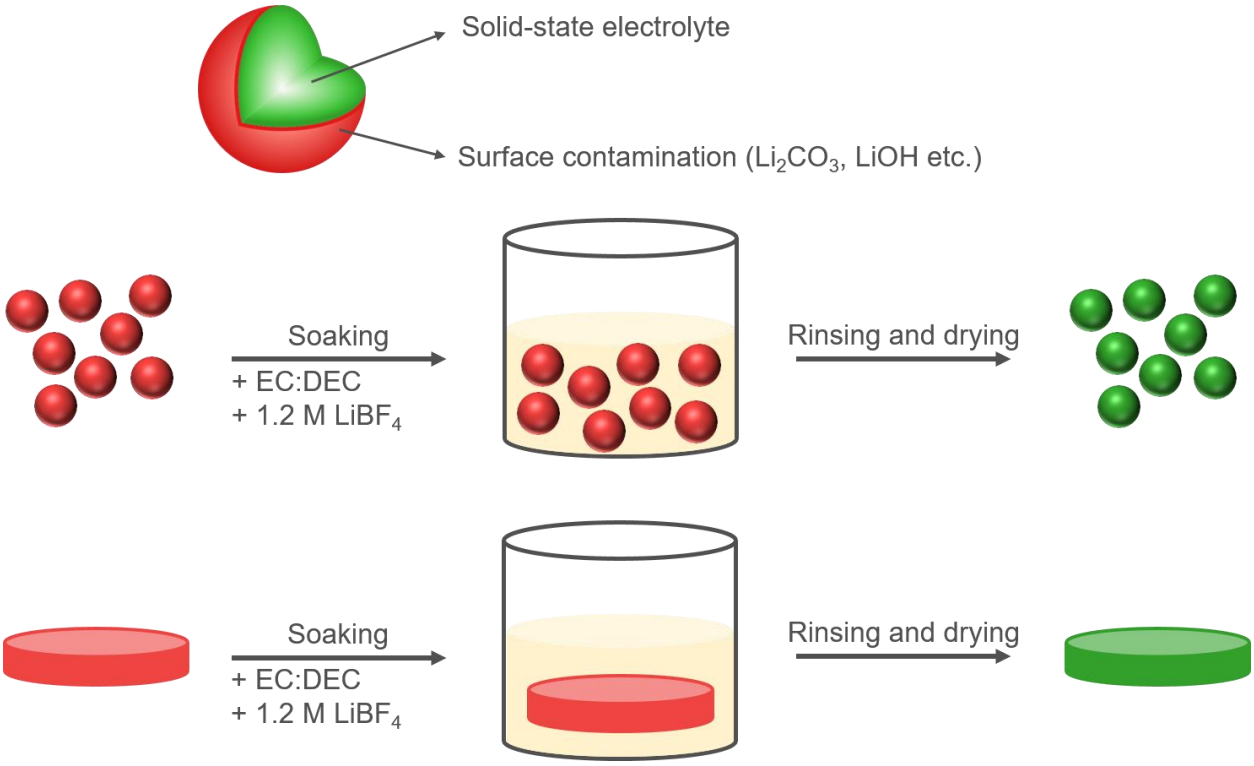

Figure 1: Schematic of the soaking and rinsing process to remove surface contaminants on SSEs in powder or pellet form. The general methodology used to clean the surface of LLZO powders and pellets involves a soaking step in lithium salt containing electrolyte, a subsequent rinsing with a lithium salt free organic solvent mixture and a final step of vacuum drying.

Results and Discussion

Several authors have previously shown, how exposure to air, i.e., CO_2 (in ambient conditions) can lead to the formation of Li_2CO_3 on the surface of LLZO.[9,19–21] Even during the synthesis of LLZO, exposure to air or using excess Li_2CO_3 precursor, which is very common to compensate for lithium loss through evaporation at high temperature, can lead to the formation of Li_2CO_3 on particle or pellet surfaces, which can be detrimental for the Li-ion transportation properties of LLZO.[21] Figure 2a shows the oxygen K-edge soft X-ray absorption spectroscopy for LLZO powder exposed to air for three days, to allow enough time for sufficient surface contaminant build-up. The soft XAS spectra for exposed LLZO powder (black), obtained using total electron yield (TEY) mode, which probes the top 5 nm, shows a clear similarity to Li_2CO_3 powder used as a standard (red). In particular, the sharp peak at 534 eV visible in the oxygen K-edge spectra, which can be assigned to the O 1s to π^*(C=O) transition,[22] indicates the presence of carbonate on the surface of LLZO powder. After soaking for 16 hours, the absorption feature for Li_2CO_3 clearly is reduced and the LLZO absorption feature at 532.3 eV (attributable to lattice oxygen in LLZO) became more prominent, suggesting the removal of Li_2CO_3. We have also used the fluorescence yield (FY) mode, which probes up to a depth of 100 nm (Figure 2b). The normalized O K-edge spectra in the FY mode (50 – 100 nm) shows a more intense absorption feature at 532.3 eV for the air-exposed LLZO than seen in the O K-edge spectra obtained using TEY mode (5 nm), indicating that the carbonate layer is less than 100 nm deep. Our results are in good agreement with what has been reported previously by Cheng et al.[9,22] In addition to the O K-edge XAS, the C K-edge and La M-edge spectra were also collected in TEY mode, and are shown in Figure 2c and Figure 2d, respectively. Two major features could be identified in the C K-edge XAS spectrum representing the transition from C 1s to σ^*(C-H) and C 1s to π^*(C=O) at 288.7 eV and 290.5 eV, respectively. The second peak at 290.5 eV confirms the presence of Li_2CO_3 on the surface of exposed LLZO powder. After soaking, a significant reduction in the absorption intensity could be seen, confirming the removal of surface Li_2CO_3 by the 16 h soaking procedure. The much lower intensity of the first peak at 288.7 eV in the Li_2CO_3 reference and the observed higher absorbance in exposed LLZO powder and cleaned LLZO powder may arise from trace carbon contaminants already present on the LLZO powder; but could also be introduced from the organic solvents used for the cleaning procedure. The efficacy of the cleaning process at removing the Li_2CO_3 layer on the surface of LLZO is apparent from Figure 2d. Using the raw intensity, which is only normalized by the incident flux, a strong increase in the La M-edge TEY signal intensity can be seen as the soaking time increased. The exposed LLZO powder prior to soaking showed a very low peak intensity, due to coverage by a carbonate layer.

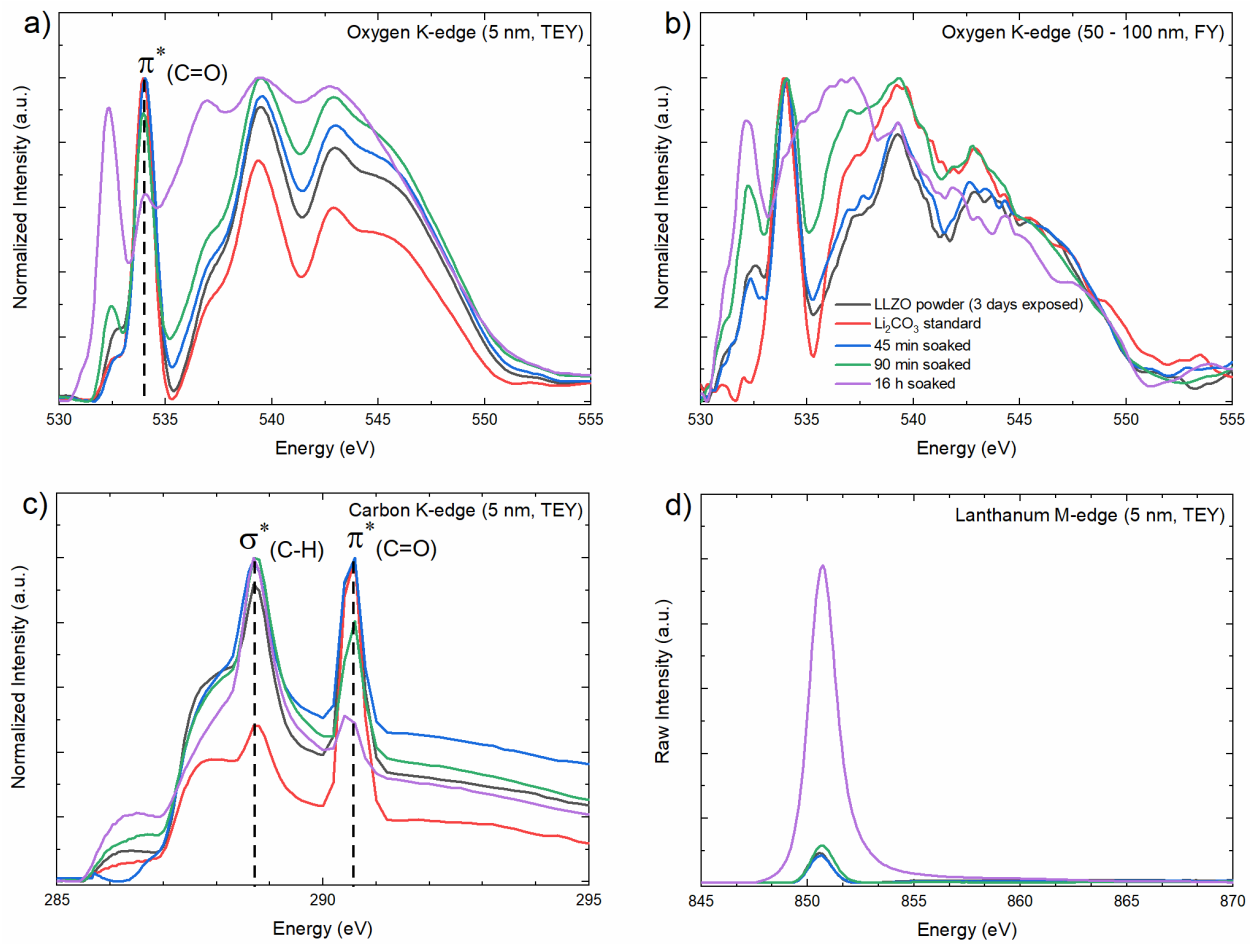

Figure 2: Soft XAS spectrum of (a) Oxygen K-edge (TEY mode), (b) Oxygen K-edge (FY mode), (c) Carbon K-edge (TEY mode), and (d) Lanthanum M-edge (TEY mode). Soaking LLZO powders for 16 hours in 1.2 M $LiBF_4$ containing EC:DEC (50:50, wt%) shows a clear reduction of the carbonate peak, also indicated by a higher intensity of the La M-edge peak (d).

A clear reduction of the carbonate layer could also be observed with Raman spectroscopy, and confirmed the results obtained using soft XAS. The LLZO phase was confirmed to be cubic, as also reported previously in the literature.[19,23] Peaks appearing in the Raman spectrum could be assigned to Zr-O bond stretching, lithium vibrations, as well as Li_2CO_3 at 1085 cm^{-1} (see dashed line in Figure 3).[19,22–24] A clear, almost complete reduction of the Li_2CO_3 peak could be observed after soaking for 16 hours in $LiBF_4$ containing organic solvent, without a change of the surface compared to the initial state. The procedure of carbonate removal by soaking was also conducted for LLZO pellets (Figure 3b). Due to the relatively smaller surface area compared to powder LLZO, the total time of air exposure was increased to 1 month. A significant carbonate signal could be observed on top of the LLZO pellets, and a total removal of the carbonate could only be achieved after soaking for 22 hours in $LiBF_4$ containing solvent.

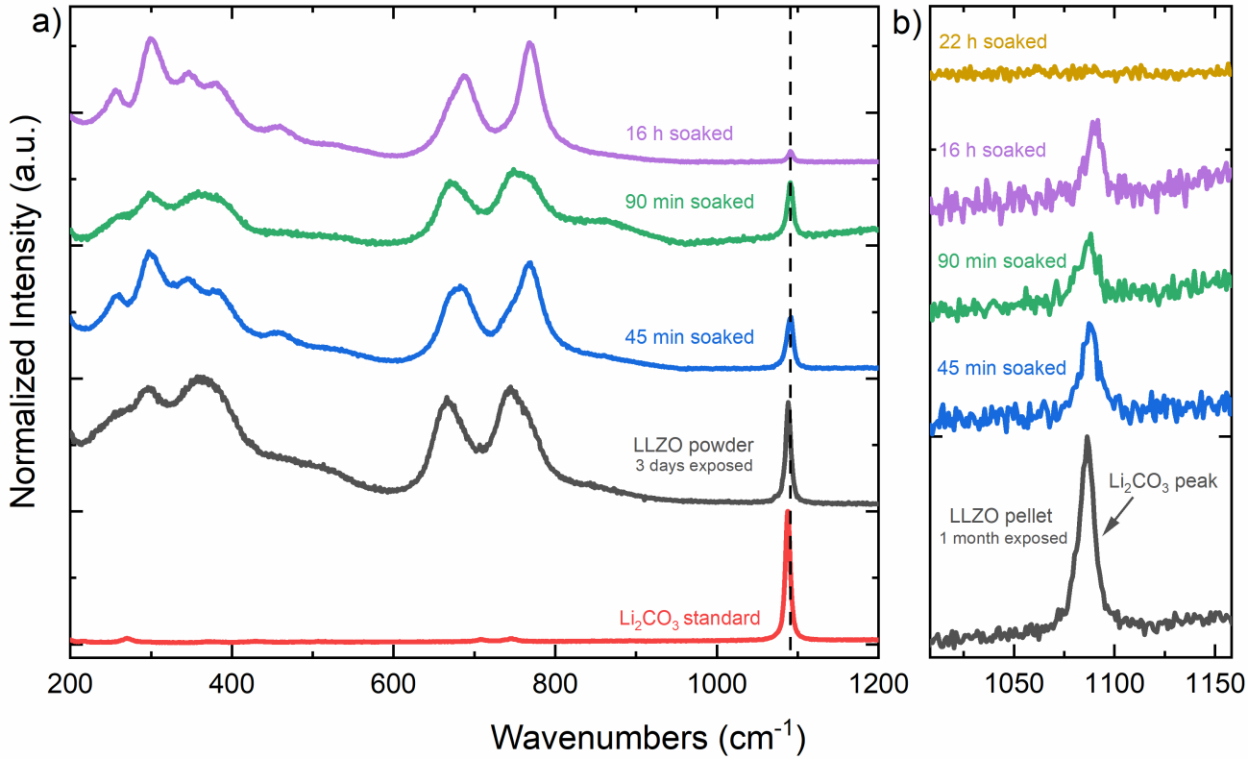

Figure 3: (a) Raman characterization of LLZO powder exposed to air and soaked for various times with 1.2 M $LiBF_4$ containing organic solvent (EC:DEC, 50:50, wt%). A clear reduction of the Li_2CO_3 vibration at 1085 cm^{-1} is indicating a removal of Li_2CO_3 after soaking for long times. (b) Carbonate peaks in LLZO pellet samples showing a complete removal of the Li_2CO_3 layer after 22 h of soaking.

The integrated peak area for the carbonate vibration at 1085 cm^{-1} was used to determine semi-quantitatively, how fast carbonate can be removed from the LLZO surface. Carbonate peak areas for samples after soaking

were normalized to the initial Li_2CO_3 peak area of the exposed LLZO samples. After 45 minutes of soaking, almost 67% of the carbonate layer was removed from the pellet's surface, while only 23% of the carbonate was removed from surfaces of the powder.

Figure 4 shows the X-ray powder diffraction (XRD) pattern of LLZO powder exposed for 3 days to air and LLZO powder subsequently soaked with $LiBF_4$ electrolyte. The XRD pattern for the exposed powder displayed reflections for both LLZO and Li_2CO_3,[25] although Li_2CO_3 peaks were much less pronounced. A similar decrease of the carbonate signatures after soaking was observed as with the soft XAS and Raman measurements and confirms its removal. Soaking with $LiBF_4$ containing electrolyte also showed that there was no effect on the crystal structure of the bulk LLZO material, i.e., LLZO is still in the cubic phase. Exposure to moisture and CO_2 is known to cause proton exchange and substitution of Li^+ with H^+ and hence leads to a phase transition in LLZO from cubic to tetragonal.[13,20] Due to the unchanged LLZO structure indicated by our XRD results, most likely this substitution of Li^+ by H^+ is happening on the surface of the LLZO samples.[13]

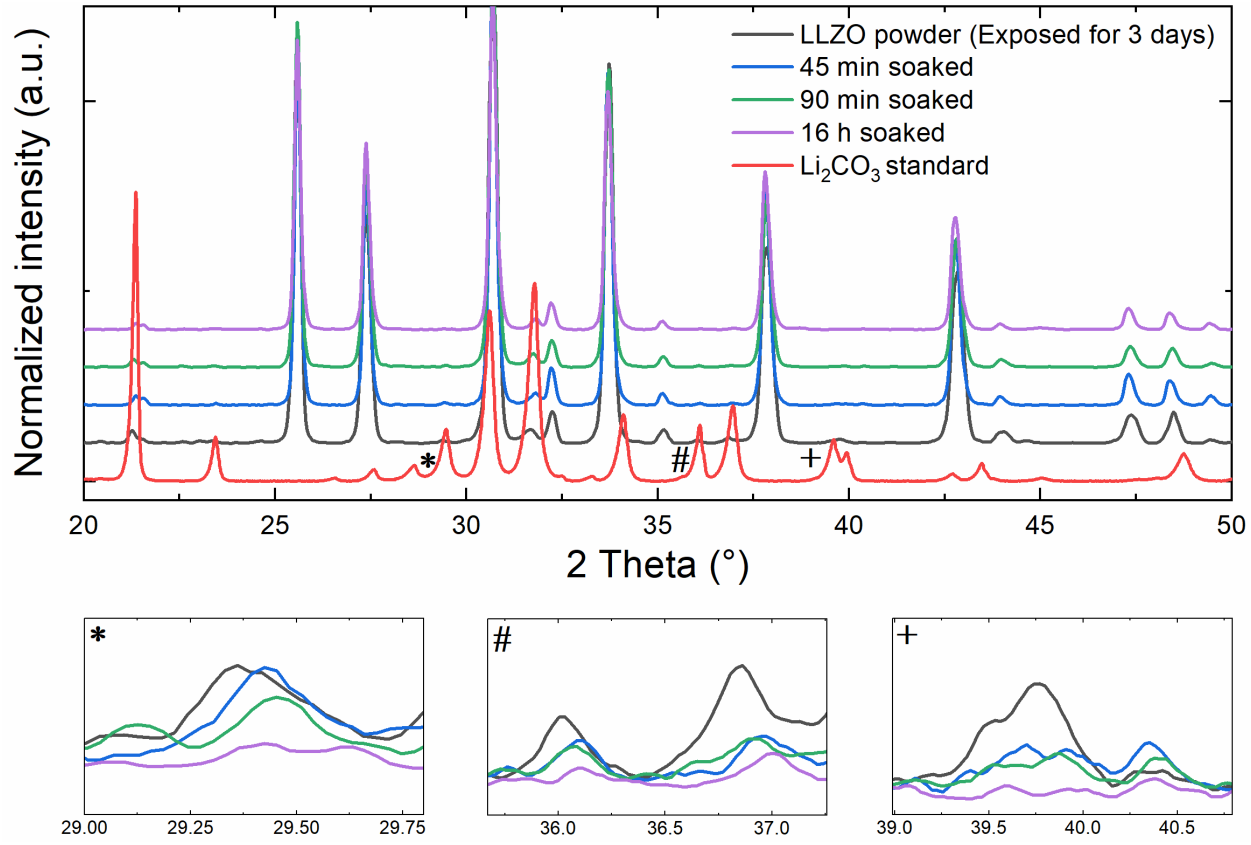

Figure 4: XRD characterization of LLZO powder exposed to air and soaked for various times with $LiBF_4$ containing organic solvent. Peaks marked with an asterisk, hashtag and plus sign are presented in separate panels and show a clear reduction of diffraction peaks associated to Li_2CO_3. Positioning of carbonate peaks is annotated with dashed lines.

To verify that the removal of Li_2CO_3 also boosts the electrochemical performance of the cleaned pellets, we built symmetric Li//LLZO//Li cells and used a simple method of lithium plating and stripping (galvanostatic cycling) as well as potentio electrochemical impedance spectroscopy (PEIS) for characterization; details on the used methodology and cell building can be found in the experimental section. Cycling lithium between the electrodes using exposed 2 mm thick LLZO pellets showed a very noisy potential and a large voltage polarization (see Figure 5a). After soaking for 16 hours, LLZO pellets sandwiched between two lithium foils stabilized at around 0.03 V (purple). In contrast to this, symmetric cells containing unsoaked pellets stabilized at around 0.15 V (black). Besides the lower voltage polarization, the cells containing the soaked pellets also cycled cleanly without much noise. Figure 5b shows Nyquist plots for cells with unsoaked LLZO pellets sandwiched between lithium. A very high initial impedance can be observed at the first cycle, which stabilized with increasing cycle number at the end of the galvanostatic cycling. In contrast to this, cells built with a soaked LLZO pellet showed an approx. 5 times lower impedance (interfacial + bulk) and a very consistent during cycling (Figure 5c). The reduction in the total impedance can be credited to the removal of the carbonate layer on top of the LLZO pellets during the soaking process. This results in more conformal contact of lithium metal on the LLZO surface, which enhances the effective ionic transfer area and transport of ions between LLZO and Li. In this work LLZO pellets of approx. 2 mm thickness were used, the as-purchased LLZO pellets are almost twice as thick or higher when comparing to other LLZO work by various authors.[22,24,26] The goal in this work was not to outperform the achievable interfacial resistance or usable critical current density by optimizing the pressure or adapting high temperatures between LLZO and lithium during cell making and electrochemical cycling as seen by other authors.[22,26] How the interfacial resistance can be reduced with additional compression, or heating during cell preparation to ensure a good contact between lithium and the LLZO pellet has already been shown in the literature.[11,26,27] Furthermore, our proposed method might not be able to re-exchange protons with Li^+ on the surface and hence has a negative impact on the impedance. Herein, a simple Hohsen 2032 coin cell setup, without any additional pressure or temperature application during cell making and cycling, was used to demonstrate the concept of electrolyte soaking for carbonate removal. How galvanostatic cycling at higher temperatures (80°C) can affect the

electrochemical impedance spectra can be seen in supplementary Figure S1, which shows a roughly 10 fold lower impedance at higher temperatures for both unsoaked and soaked LLZO pellets.

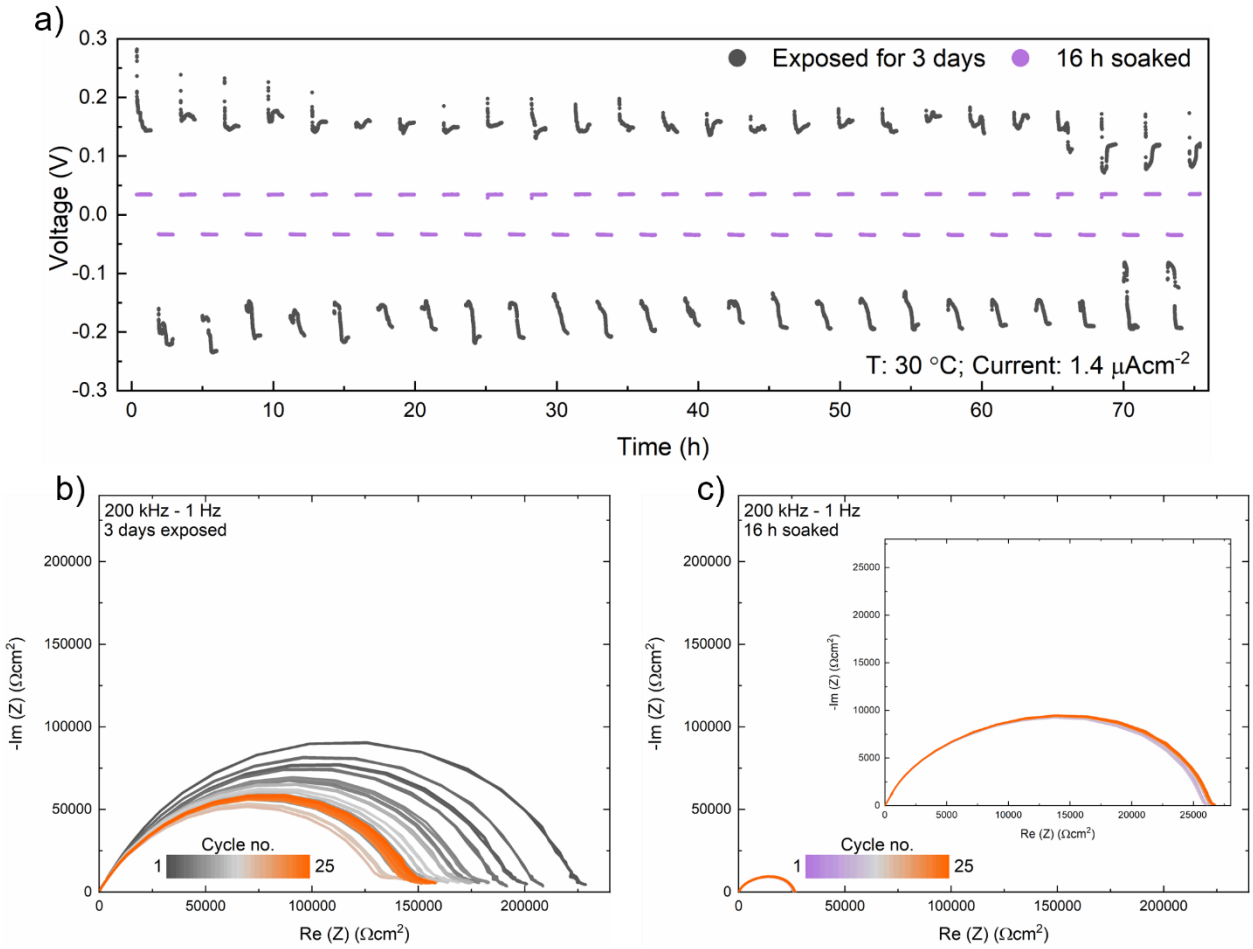

Figure 5: (a) Galvanostatic cycling of symmetric Li//LLZO//Li cells at 30°C with LLZO pellets exposed to air (black) and soaked for 16 hours (purple). Electrochemical impedance spectra by cycle (black to orange) for symmetric cells with exposed LLZO and (c) electrochemical impedance spectra by cycle (purple to orange) for 16 h soaked LLZO with the same scale as (b) to see the reduction in impedance. The inset is showing how close together the impedance spectra are in comparison to the unsoaked pellets.

Several reaction mechanism have been proposed in the literature to understand how Li_2CO_3 is removed upon addition of $LiBF_4$.[28,29] Both of these mechanisms are similar to the reactions of $LiPF_6$ salt observed in Li-ion batteries. The first reaction mechanism involves the reaction of $LiBF_4$ with trace amounts of water to form HF and BF_3 which in turn further react with Li_2CO_3 to form LiF, CO_2 and LiOH (Equation 1-3).

$$LiBF_4 + H_2O \rightleftharpoons LiOH + HF + BF_3 \qquad (1)$$

$$HF + Li_2CO_3 \rightleftharpoons LiF + LiOH + CO_{2(g)} \quad (2)$$

$$BF_3 + Li_2CO_3 \rightleftharpoons 2LiF + CO_{2(g)} + BOF_{(g)} \quad (3)$$

The second mechanism involves a direct reaction of Li_2CO_3 with $LiBF_4$ to form LiF, CO_2 and BOF gas similar to the POF_3 gas formed between reaction of $LiPF_6$ and Li_2CO_3 (Equation 4)

$$LiBF_4 + Li_2CO_3 \rightleftharpoons 3LiF + CO_{2(g)} + BOF_{(g)} \quad (4)$$

Using thermodynamic data for standard enthalpy and entropy from the NIST database[30] and the Materials Project[31] we calculated the free energy change (ΔG) associated with the above reactions. We found that reactions 1, 2 and 3 have a positive ΔG, which implies that these reactions would be improbable and the mechanisms proposed above are unlikely. This is because BF_3, HF, and BOF are highly unstable molecules. Herein we propose a different reaction mechanism (Equation 5).

$$2LiBF_4 + 3Li_2CO_3 \rightleftharpoons 8LiF + 3CO_{2(g)} + B_2O_{3(s)} \quad (5)$$

The ΔG associated with this reaction is -110.85 kJ/mol making this reaction highly likely. To see whether the solid LiF is washed away from the surface, we have analyzed the surface of cleaned LLZO pellets with soft XAS. Using the fluorine K-edge signal and comparing the spectrum to LiF powder, a clear similarity can be seen (supplementary Figure S2). This result indicates that some of the formation products during Li_2CO_3 decomposition remain on the surface of cleaned LLZO, and might not be washed away, even if the solution is stirred. A layer of LiF could also prevent the exchange of protons in Li^+ sites, an effect of further exposure to moisture and CO_2.

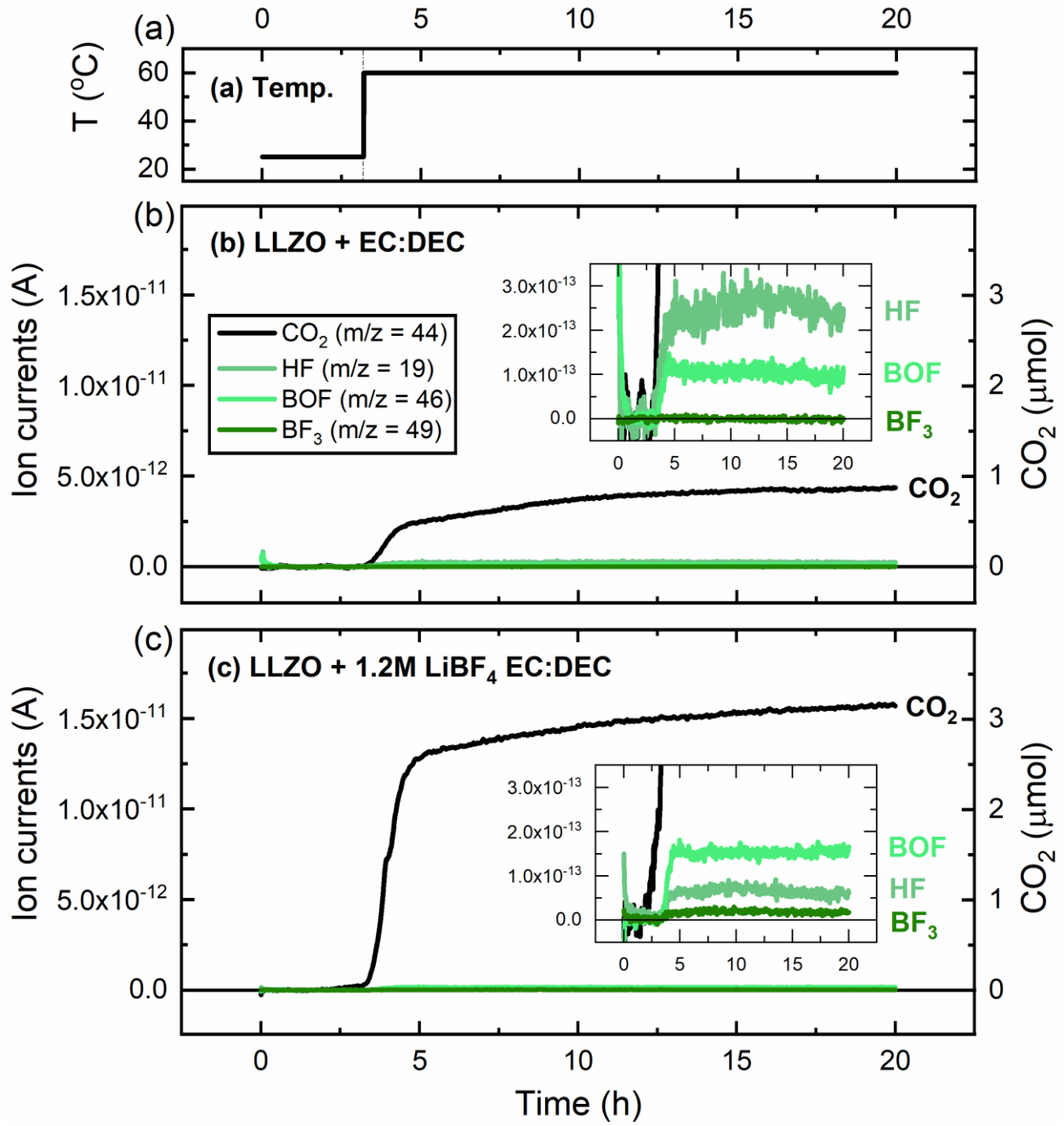

Figure 6: On-line mass spectrometry (OMS) temperature stepping experiment. (a) Temperature set points at 25 and 60°C. (b) Ion current signals from the OMS cell during exposure of air-exposed LLZO powder to EC:DEC solvent mixture without $LiBF_4$; (c) Ion current signals during exposure of air-exposed LLZO powder to $LiBF_4$ containing EC:DEC electrolyte showing trice the amount of CO_2.

We confirmed that CO_2 is the major reaction gas evolved when mixing air exposed LLZO powder with $LiBF_4$ containing electrolyte in a temperature stepping experiment (see Figure 6b and c, and

supplementary Figure S3-4 for the survey scan) using on-line mass spectrometry (OMS). In a control experiment, the same powder was exposed to the EC:DEC solvent mix only (no $LiBF_4$). The cumulative CO_2 concentration in the custom OMS cell amounted to 3.2 µmol CO_2 when $LiBF_4$ was present (Figure 6c). When LLZO is only mixed with carbonate solvents less than a third of that CO_2 generation was observed (Figure 6b). Our free energy calculations suggest that in the case of $LiBF_4$ containing electrolyte CO_2 is likely generated according to Equation 5. The CO_2 concentration in the absence of $LiBF_4$ containing electrolyte can likely be explained by the hydrolysis of the EC solvent with either residual H_2O in the electrolyte or OH-surface groups on the exposed oxide surface. H_2O and OH-drive EC hydrolysis at various temperatures as has been recently quantified on transition metal oxide surfaces.[32,33] Using the CO_2 concentration difference in Figure 6b, that likely stems from the reaction depicted in Equation 5, we can estimate the amount of carbonate surface coverage on the LLZO particles. Supplementary table 1 shows that a 10 nm layer of carbonate on the LLZO particles (88.78 mg powder with surface area of 0.1 m^2/g) would be sufficient to explain ~83% of the CO_2 generation measured via OMS. As a check, we can compare the amount of carbonate that can be converted to CO_2 from the total amount of $LiBF_4$ supplied in solution. We see that $LiBF_4$ is supplied in a >200-fold excess and thus all surface carbonate should be converted to CO_2, especially at 60°C. Insets in Figure 6b and c show that insignificant amounts of HF, BOF or BF_3 were generated, which further corroborates the reaction mechanism suggested by our free energy calculations.

Our free energy calculations also suggest that $LiBF_4$ favorably reacts with LiOH (ΔG = -490 kJ/mol) forming LiF and a soluble product $LiB(OH)_4$ (Equation 6), which aids in cleaning the LLZO surface.

$$LiBF_4 + 4LiOH \rightleftharpoons 4LiF + LiB(OH)_4 \qquad (6)$$

Since $LiBF_4$, is an expensive salt, we suggest that $NaBF_4$ and KBF_4 can also be used as cheaper alternatives for LLZO surface cleaning. Free energy calculations, as depicted in supplementary Equation (S1-S9), make the proposed reactions for surface cleaning with $NaBF_4$ and KBF_4 likely.

Conclusions

In this work, we have used a simple, easily scalable, non-destructive, and non-mechanical methodology to remove the Li_2CO_3 layer, which forms upon exposure to air from the surface of LLZO. By simply soaking LLZO powders and pellets in $LiBF_4$ containing liquid electrolyte solution of EC and DEC for a certain period, total removal of carbonate could be achieved as confirmed by soft XAS, Raman spectroscopy, and XRD. Additional galvanostatic cycling and electrochemical impedance spectroscopy experiments confirmed that removing the lithium carbonate resulted in a lower impedance by a factor of ~8.5 as well as significantly lower voltage polarization. Via on-line mass spectrometry and free energy calculations we identified that the direct reaction of $LiBF_4$ with surface Li_2CO_3 estimated to be about ~10 nm thick results in gaseous CO_2 and soluble B_2O_3, and LiF. This simple technique can be easily applied to powders, hybrid polymer/ceramic structures or the extremely thin SSE films needed for real cells, which are too fragile to withstand polishing or other brute force methods of removing lithium carbonate, and is especially suited for removing Li_2CO_3 layers due to usage of excess Li_2CO_3 precursors.

Experimental Section

Soaking procedure

LLZO powder and LLZO pellets (from the same commercial source) 12 mm in diameter with a thickness of 1.95 – 2.00 mm were exposed to air for 3 days in a fume hood. After exposure and initial characterization of the carbonate layer, the samples were transferred into an argon filled glovebox (O_2 < 0.1 ppm, H_2O < 0.1 ppm). Powders and pellets were soaked individually at room temperature for 45 minutes, 90 minutes and 16 hours with 20 mL of 1.2 M $LiBF_4$ in ethylene carbonate (EC):diehtyl carbonate (DEC) (50:50, wt%). The whole solution was stirred using a small stir bar of 14 mm length and a magnetic stirrer. After soaking for the respective time periods, the powders and pellets were rinsed using a EC:DEC (50:50, wt%) solvent mix. Cleaned LLZO powder was centrifuged and the supernatant was decanted. Powders and pellets were vacuum dried at room temperature in the glove box antechamber for 5 hours prior to characterization.

Soft XAS synchrotron characterization

Thin layers of exposed and cleaned LLZO powder samples were spread onto a conductive carbon tape, which was then attached to an aluminum sample holder inside an argon filled glovebox (O_2 < 0.1 ppm, H_2O < 0.1 ppm). In a similar manner, exposed and cleaned LLZO pellets were attached to a conductive carbon tape and then onto the sample rod. The prepared aluminum rod was then packed in a pouch bag and double sealed inside the glove box prior to transportation to the experimental beam line station. Transfer into the ultrahigh vacuum chamber was done under argon atmosphere to prevent any exposure to air. Soft XAS spectra of the oxygen K-edge, carbon K-edge and lanthanum M-edge were obtained at the 31-pole wiggler beamline 10-1 at the Stanford Synchrotron Radiation Lightsource (SSRL) with a spherical grating monochromator with 20 mm entrance and exit slits, a 0.2 eV energy resolution and a 2 x 2 mm beam spot. Data collection was performed under ultrahigh vacuum (10^{-9} Torr) at room temperature. All data were collected in a single load using the total electron yield (TEY) and fluorescence yield (FY) mode detectors. Data was processed using the Python multichannel analyzer (PyMCA) software of the European Synchrotron Radiation Facility (ESRF).[34]

Raman spectroscopic characterization

Raman spectroscopy was conducted using a Horiba Scientific LabRAM HR Evolution Raman microscope equipped with a 405 nm diode laser, a 1800 grooves per mm grating, and a Synapse

Open-Electrode CCD detector. The laser was focused using an Olympus lens with 50 x magnification, a numerical aperture (NA) of 0.5, and a field number of 26.5. An area of approx. 60 x 80 µm was probed by the laser. Scattered radiation was collected in a backscattering geometry through the same lens. Rayleigh-scattered laser light was removed using a filter prior hitting the spectrometer. Several spots were measured and averaged to assure representative spectra collection. Spectra were collected between 0 and 1200 cm^{-1} and an acquisition time of 60 seconds for each spot.

XRD characterization

Powder X-ray diffraction patterns were recorded using a Bruker D8 ADVANCE X-ray diffractometer equipped with a Cu K-α radiation source. The accelerating voltage and current were 40 kV and 40 mA, respectively. Scans were collected between 10 and 55° (2θ) at a scan speed of 0.02°/s and a step size of 0.01°.

Electrochemical characterization

For the symmetric Li//LLZO//Li cells, exposed or cleaned LLZO pellets were sandwiched between high-purity Honjo lithium foil 60 µm thick 10 mm in diameter in an argon filled glovebox (O_2 < 0.1 ppm, H_2O < 0.1 ppm) using Hohsen 2032 coin cells and two 0.5 nm stainless steel spacers. Several Li//LLZO//Li cells were built using exposed as well as exposed and soaked LLZO pellets. Lithium plating and stripping experiments were carried out at a current density of 1.4 $\mu A/cm^2$ using a BioLogic VMP3 potentiostat. A low current density was used, since the measurements were conducted at room temperature and without high compression. After 30 minutes of plating, a 30 minute rest step was used prior to collecting electrochemical impedance spectra (from 200 kHz to 1 Hz). Subsequently, a 30 minute lithium stripping step was carried out, followed by a 30 minute rest step and another PEIS step was performed. All experiments were conducted at 30°C in a temperature controlled environment.

On-line mass spectrometry

Gas generation from LLZO exposure to $LiBF_4$ containing electrolyte was quantified by on-line mass spectrometry. LLZO powder that had been air exposed for three days prior to measurement was mixed with 1.2M $LiBF_4$ EC:DEC electrolyte in a custom mass spectrometry cell that is connected to a custom-built on-line mass spectrometry setup. In a control experiment, the same powder was exposed to the EC:DEC solvent mix only (no $LiBF_4$). The gases generated from the

reaction are reported in µmol of cumulative gas concentration in the reaction vessel using a calibration gas that contains 2000 ppm of H_2, C_2H_4, O_2 and CO_2 in Ar. Gas concentrations were converted into mols of gas using the cell volume of 18 ml, the ideal gas law, and the respective molar mass of the gas molecule. Gases that are not present in the calibration gas are reported as ion current signals at the secondary electron multiplier and their amounts can be compared on a semi-quantitative basis.

Acknowledgements

The synchrotron experiments of this research were performed at the Stanford Synchrotron Radiation Lightsource (SSRL), a Directorate of SLAC National Accelerator Laboratory and an Office of Science User Facility operated for the U.S. Department of Energy Office of Science by Stanford University. Use of the Stanford Synchrotron Radiation Lightsource, SLAC National Accelerator Laboratory, is supported by the U.S. Department of Energy, Office of Science, Office of Basic Energy Sciences under Contract DE-AC02-76SF00515. Work at the Molecular Foundry was supported by the Office of Science, Office of Basic Energy Sciences, of the U.S. Department of Energy under Contract DE-AC02-05CH11231.

References

(1) Ramakumar, S.; Deviannapoorani, C.; Dhivya, L.; Shankar, L. S.; Murugan, R. Lithium Garnets: Synthesis, Structure, Li+ Conductivity, Li+ Dynamics and Applications. *Prog. Mater. Sci.* **2017**, *88*, 325–411. https://doi.org/10.1016/j.pmatsci.2017.04.007.

(2) Teng, S.; Tan, J.; Tiwari, A. Recent Developments in Garnet Based Solid State Electrolytes for Thin Film Batteries. *Curr. Opin. Solid State Mater. Sci.* **2014**, *18* (1), 29–38. https://doi.org/10.1016/j.cossms.2013.10.002.

(3) Cao, C.; Li, Z.-B.; Wang, X.-L.; Zhao, X.-B.; Han, W.-Q. Recent Advances in Inorganic Solid Electrolytes for Lithium Batteries. *Front. Energy Res.* **2014**, *2* (June), 1–10. https://doi.org/10.3389/fenrg.2014.00025.

(4) Manthiram, A.; Yu, X.; Wang, S. Lithium Battery Chemistries Enabled by Solid-State Electrolytes. *Nat. Rev. Mater.* **2017**, *2* (4), 1–16. https://doi.org/10.1038/natrevmats.2016.103.

(5) Albertus, P.; Babinec, S.; Litzelman, S.; Newman, A. Status and Challenges in Enabling the Lithium Metal Electrode for High-Energy and Low-Cost Rechargeable Batteries. *Nat. Energy* **2018**, *3* (1), 16–21. https://doi.org/10.1038/s41560-017-0047-2.

(6) Zu, C.; Azimi, N.; Zhang, Z.; Manthiram, A. Insight into Lithium–Metal Anodes in Lithium–Sulfur Batteries with a Fluorinated Ether Electrolyte. *J. Mater. Chem. A* **2015**, *3* (28), 14864–14870. https://doi.org/10.1039/C5TA03195H.

(7) Liu, B.; Xu, W.; Zhang, J.-G. Stabilization of Lithium-Metal Anode in Rechargeable Lithium-Air Batteries. In *Metal-Air Batteries*; Wiley-VCH Verlag GmbH & Co. KGaA: Weinheim, Germany, 2018; pp 11–40. https://doi.org/10.1002/9783527807666.ch2.

(8) Chang, Z.; Wang, X.; Yang, Y.; Gao, J.; Li, M.; Liu, L.; Wu, Y. Rechargeable Li//Br Battery: A Promising Platform for Post Lithium Ion Batteries. *J. Mater. Chem. A* **2014**, *2* (45), 19444–19450. https://doi.org/10.1039/C4TA04419C.

(9) Cheng, L.; Crumlin, E. J.; Chen, W.; Qiao, R.; Hou, H.; Franz Lux, S.; Zorba, V.; Russo, R.; Kostecki, R.; Liu, Z.; et al. The Origin of High Electrolyte–Electrode Interfacial Resistances in Lithium Cells Containing Garnet Type Solid Electrolytes. *Phys. Chem.*

Chem. Phys. **2014**, *16* (34), 18294–18300. https://doi.org/10.1039/C4CP02921F.

(10) Sharafi, A.; Meyer, H. M.; Nanda, J.; Wolfenstine, J.; Sakamoto, J. Characterizing the Li-Li7La3Zr2O12interface Stability and Kinetics as a Function of Temperature and Current Density. *J. Power Sources* **2016**, *302*, 135–139. https://doi.org/10.1016/j.jpowsour.2015.10.053.

(11) Cheng, L.; Chen, W.; Kunz, M.; Persson, K.; Tamura, N.; Chen, G.; Doeff, M. Effect of Surface Microstructure on Electrochemical Performance of Garnet Solid Electrolytes. *ACS Appl. Mater. Interfaces* **2015**, *7* (3), 2073–2081. https://doi.org/10.1021/am508111r.

(12) Sharafi, A.; Yu, S.; Naguib, M.; Lee, M.; Ma, C.; Meyer, H. M.; Nanda, J.; Chi, M.; Siegel, D. J.; Sakamoto, J. Impact of Air Exposure and Surface Chemistry on Li–Li 7 La 3 Zr 2 O 12 Interfacial Resistance. *J. Mater. Chem. A* **2017**, *5* (26), 13475–13487. https://doi.org/10.1039/C7TA03162A.

(13) Cheng, L.; Liu, M.; Mehta, A.; Xin, H.; Lin, F.; Persson, K.; Chen, G.; Crumlin, E. J.; Doeff, M. Garnet Electrolyte Surface Degradation and Recovery. *ACS Appl. Energy Mater.* **2018**, *1* (12), 7244–7252. https://doi.org/10.1021/acsaem.8b01723.

(14) Li, Y.; Chen, X.; Dolocan, A.; Cui, Z.; Xin, S.; Xue, L.; Xu, H.; Park, K.; Goodenough, J. B. Garnet Electrolyte with an Ultralow Interfacial Resistance for Li-Metal Batteries. *J. Am. Chem. Soc.* **2018**, *140* (20), 6448–6455. https://doi.org/10.1021/jacs.8b03106.

(15) Han, X.; Gong, Y.; Fu, K.; He, X.; Hitz, G. T.; Dai, J.; Pearse, A.; Liu, B.; Wang, H.; Rubloff, G.; et al. Negating Interfacial Impedance in Garnet-Based Solid-State Li Metal Batteries. *Nat. Mater.* **2017**, *16* (5), 572–579. https://doi.org/10.1038/nmat4821.

(16) Gutiérrez-Pardo, A.; Pitillas Martinez, A. I.; Otaegui, L.; Schneider, M.; Roters, A.; Llordés, A.; Aguesse, F.; Buannic, L. Will the Competitive Future of Solid State Li Metal Batteries Rely on a Ceramic or a Composite Electrolyte? *Sustain. Energy Fuels* **2018**, *2* (10), 2325–2334. https://doi.org/10.1039/C8SE00273H.

(17) Kanamura, K.; Tamura, H.; Shiraishi, S.; Takehara, Z. XPS Analysis of Lithium Surfaces Following Immersion in Various Solvents Containing LiBF4. *J. Electrochem. Soc.* **1995**, *142* (2), 340–347.

(18) Aurbach, D.; Ein-Eli, Y.; Zaban, A. The Surface Chemistry of Lithium Electrodes in Alkyl Carbonate Solutions. *J. Electrochem. Soc.* **1994**, *141* (1), L1–L3.

(19) Larraz, G.; Orera, A.; Sanjuán, M. L. Cubic Phases of Garnet-Type Li7La3Zr2O12: The Role of Hydration. *J. Mater. Chem. A* **2013**, *1* (37), 11419. https://doi.org/10.1039/c3ta11996c.

(20) Wang, Y.; Lai, W. Phase Transition in Lithium Garnet Oxide Ionic Conductors Li7La3Zr2O12: The Role of Ta Substitution and H2O/CO2 Exposure. *J. Power Sources* **2015**, *275*, 612–620. https://doi.org/10.1016/j.jpowsour.2014.11.062.

(21) Wagner, R.; Rettenwander, D.; Redhammer, G. J.; Tippelt, G.; Sabathi, G.; Musso, M. E.; Stanje, B.; Wilkening, M.; Suard, E.; Amthauer, G. Synthesis, Crystal Structure, and Stability of Cubic Li7-XLa3Zr2-XBixO12. *Inorg. Chem.* **2016**, *55* (23), 12211–12219. https://doi.org/10.1021/acs.inorgchem.6b01825.

(22) Cheng, L.; Wu, C. H.; Jarry, A.; Chen, W.; Ye, Y.; Zhu, J.; Kostecki, R.; Persson, K.; Guo, J.; Salmeron, M.; et al. Interrelationships among Grain Size, Surface Composition, Air Stability, and Interfacial Resistance of Al-Substituted Li 7 La 3 Zr 2 O 12 Solid Electrolytes. *ACS Appl. Mater. Interfaces* **2015**, *7* (32), 17649–17655. https://doi.org/10.1021/acsami.5b02528.

(23) Tietz, F.; Wegener, T.; Gerhards, M. T.; Giarola, M.; Mariotto, G. Synthesis and Raman Micro-Spectroscopy Investigation of Li7La3Zr2O12. *Solid State Ionics* **2013**, *230* (C), 77–82. https://doi.org/10.1016/j.ssi.2012.10.021.

(24) Han, F.; Yue, J.; Chen, C.; Zhao, N.; Fan, X.; Ma, Z.; Gao, T.; Wang, F.; Guo, X.; Wang, C. Interphase Engineering Enabled All-Ceramic Lithium Battery. *Joule* **2018**, *2* (3), 497–508. https://doi.org/10.1016/j.joule.2018.02.007.

(25) Vardar, G.; Bowman, W. J.; Lu, Q.; Wang, J.; Chater, R. J.; Aguadero, A.; Seibert, R.; Terry, J.; Hunt, A.; Waluyo, I.; et al. Structure, Chemistry, and Charge Transfer Resistance of the Interface between Li 7 La 3 Zr 2 O 12 Electrolyte and LiCoO 2 Cathode. *Chem. Mater.* **2018**, *30* (18), 6259–6276. https://doi.org/10.1021/acs.chemmater.8b01713.

(26) Sharafi, A.; Kazyak, E.; Davis, A. L.; Yu, S.; Thompson, T.; Siegel, D. J.; Dasgupta, N.

P.; Sakamoto, J. Surface Chemistry Mechanism of Ultra-Low Interfacial Resistance in the Solid-State Electrolyte Li7La3Zr2O12. *Chem. Mater.* **2017**, *29* (18), 7961–7968. https://doi.org/10.1021/acs.chemmater.7b03002.

(27) Sharafi, A.; Yu, S.; Naguib, M.; Lee, M.; Ma, C.; Meyer, H. M.; Nanda, J.; Chi, M.; Siegel, D. J.; Sakamoto, J. Impact of Air Exposure and Surface Chemistry on Li-Li7La3Zr2O12interfacial Resistance. *J. Mater. Chem. A* **2017**, *5* (26), 13475–13487. https://doi.org/10.1039/c7ta03162a.

(28) Andersson, A. M.; Herstedt, M.; Bishop, A. G.; Edström, K. The Influence of Lithium Salt on the Interfacial Reactions Controlling the Thermal Stability of Graphite Anodes. *Electrochim. Acta* **2002**, *47* (12), 1885–1898. https://doi.org/10.1016/S0013-4686(02)00044-0.

(29) Kanamura, K.; Tamura, H.; Shiraishi, S.; Takehard, Z. I. XPS Analysis of Lithium Surfaces Following Immersion in Various Solvents Containing LiBF4. *J. Electrochem. Soc.* **1995**, *142* (2), 340–347. https://doi.org/10.1149/1.2044000.

(30) Acree, W.; Chickos, J. S. Phase Transition Enthalpy Measurements of Organic and Organometallic Compounds. Sublimation, Vaporization and Fusion Enthalpies From 1880 to 2015. Part 1. C 1 − C 10. *J. Phys. Chem. Ref. Data* **2016**, *45* (3), 033101. https://doi.org/10.1063/1.4948363.

(31) Jain, A.; Ong, S. P.; Hautier, G.; Chen, W.; Richards, W. D.; Dacek, S.; Cholia, S.; Gunter, D.; Skinner, D.; Ceder, G.; et al. Commentary: The Materials Project: A Materials Genome Approach to Accelerating Materials Innovation. *APL Mater.* **2013**, *1* (1), 011002. https://doi.org/10.1063/1.4812323.

(32) Sicklinger, J.; Metzger, M.; Beyer, H.; Pritzl, D.; Gasteiger, H. A. Ambient Storage Derived Surface Contamination of NCM811 and NCM111: Performance Implications and Mitigation Strategies. *J. Electrochem. Soc.* **2019**, *166* (12), A2322–A2335. https://doi.org/10.1149/2.0011912jes.

(33) Metzger, M.; Strehle, B.; Solchenbach, S.; Gasteiger, H. A. Hydrolysis of Ethylene Carbonate with Water and Hydroxide under Battery Operating Conditions. *J.*

Electrochem. Soc. **2016**, *163* (7), A1219–A1225. https://doi.org/10.1149/2.0411607jes.

(34) Solé, V. A.; Papillon, E.; Cotte, M.; Walter, P.; Susini, J. A Multiplatform Code for the Analysis of Energy-Dispersive X-Ray Fluorescence Spectra. *Spectrochim. Acta - Part B At. Spectrosc.* **2007**, *62* (1), 63–68. https://doi.org/10.1016/j.sab.2006.12.002.